ELSEVIER

Bone 40 (2007) 1635–1642

BONE

www.elsevier.com/locate/bone

Allometric scaling and biomechanical behavior of the bone tissue: An experimental intraspecific investigation

Stefano Z.M. Brianza [a,*], Patrizia D'Amelio [a], Nicola Pugno [b], Marco Delise [c], Cristina Bignardi [c], Giancarlo Isaia [a]

[a] *Department of Internal Medicine, C.so Dogliotti 14, 10126 Torino, Italy*
[b] *Department of Structural Engineering and Geotechnics, Politecnico di Torino, Italy*
[c] *Department of Mechanics, Politecnico di Torino, Italy*

Received 13 July 2006; revised 5 February 2007; accepted 7 February 2007
Available online 23 February 2007

Abstract

Introduction: Adaptation of bone to different loads has received much attention. This paper examines the consequences of differences in size on bones from the same animal species.
Methods: The study was conducted on 32 canine radii. Their geometry, densitometry and mechanical properties were determined and one-way ANOVA was used to analyze their distribution by sex. Bending failure was observed during the mechanical test. The bones were then likened to thin beams and the mechanical parameters of interest were appraised via beam theory. A multiple linear regression model with stepwise analyses was employed to determine which parameters rule the mechanical characteristics. The relationships between the bone mass and the parameters investigated were analyzed by means of a model II regression in order to state how the scaling of the bone characteristics act on its mechanical behavior.
Results: The linear regression model demonstrated that an animal's mass, its sex and the mineral content and the geometrical properties of its bones almost entirely predict their mechanical behavior. A close fit was found between the experimentally determined and the theoretical slopes of the log regressed allometric equations. The work to failure was found to scale almost linearly with the animal and bone mass and the macroscopical bone material properties were found to be mass invariant. The allometric equations showed that as the animal mass increases, employing proportionally the same amount of tissue, bones get proportionally shorter and proportionally distribute their tissue further from the cross-sectional centroid.
Conclusions: Our results suggest that dimensional analysis on the assumption of geometrical self-similarity and mechanical testing according to classic elastic solutions are reasonable in bones tested in accordance to our set up. The bone geometry is the parameter able to curb the energy effects of an animal mass increase. The allometric scaling of the bone length and the cross-sectional layout, without an increase in the amount of material proportionally employed, preserves linear with the animal mass the amount of energy necessary to fracture a bone and restrain the rise of stresses and strains in the cross-section.

Keywords: Biomechanics; Scaling; Bone mineral density; Bone geometry; Canine

Introduction

The relationship of body size to the anatomical, physiological, behavioral and ecological characteristics of living organisms has long been extensively investigated in biology [3,4,6,14–18,24,25,27,31,33,35,40–42,44–47,51,53,54,62–64]. Early in the twentieth century, the great biologists, D' Arcy Thompson, Cecil Murray and Julian Huxley produced influential works [33,46,55] on scaling. They considered a wide range of size-related phenomena and tried to explain them in terms of physical principles of mechanics and geometric relationships. In interpreting scaling relationships as optimal solutions to problems of mechanical design, these early studies laid the foundation of the modern discipline of biomechanics [19].

* Corresponding author. Fax: +39 0116634751.
E-mail addresses: stefanobrianza@yahoo.it (S.Z.M. Brianza), patrizia.damelio@unito.it (P. D'Amelio), nicola.pugno@polito.it (N. Pugno), marcodelise@yahoo.com (M. Delise), cristina.bignardi@polito.it (C. Bignardi), giancarlo.isaia@unito.it (G. Isaia).

8756-3282/$ - see front matter © 2007 Elsevier Inc. All rights reserved.
doi:10.1016/j.bone.2007.02.013

The principle underlying all the theoretical and quantitative studies on scaling is that changes in the size of a physical or biological system require adjustment of the relations between its components and processes to enable it to continue to function. The physical principles that rule the development and behavior of the components and processes are universal, but the biological consequences depend on the size of the organism [20]. West et al. proposed [63] these regulating principles as the rates at which energy and materials can be distributed between surfaces where they are exchanged and tissue where they are used, assuming invariant the terminal units in their distribution networks. The consequences of an organism size increase are basically related to the trend of the surface to volume ratio and to the associated production and wasting of energy.

Three principles govern the design of a biological system: interrelated exponents, invariant quantities and symmorphosis [62]. The interrelated exponents are those which fit the allometric equations that state the relations between two parameters of interest. A typical allometric equation has the form $Y = Y_0 M^b$, where Y is some dependent variable, Y_0 is a normalization constant, M is the body mass and b is the scaling exponent. The invariant quantities are the characteristics that vary as M^0. Examples across mammals are the radius of the capillaries and velocity and pressure in both the aorta and capillaries [36,37]. Symmorphosis is the observed tendency of biological structures to develop so as to meet, but not exceed the maximal demand [62]. These scaling relations reflect solutions whose sole purpose is to meet the maximum requirements.

Scaling of the musculoskeletal design of terrestrial animals and its adaptation to mechanical constraints of size have also been investigated in intraspecific [22,60] interorder [26,49,50,52] and mostly in interspecific studies [2,5,9,10,11,13,23,28,29,30,34,40,43,56,58]. Due to the different scaling of surface and volume as the body size increases, the energy to be controlled by the bearing framework during physiological activities scales faster than parameters favorable to the avoidance of fractures. Investigation of the extent to which the geometrical [7], the densitometric and the mechanical properties of bone scale with increases in the size of an animal in a given species gives an idea of the strategies adopted by its tissue to adjust its structure and function to compensate for the geometrical, physical and biological consequences of differences in size.

This study assesses the bone material and structural characteristics and mechanical behavior of different sized canine radii in an illustration of the relations between the size of a bone, its morphology and mechanical behavior in terms of the parameters that are the rulers of the mechanical function.

Materials and methods

Experimental model

Thirty-two pairs of radius and ulna were obtained from fully grown dogs (age 9.7±4.7 years, 18 F, 14 M, body mass 14.6±12.2 kg: 1.6–45 kg) that died naturally or euthanized due to causes unaffecting bone integrity. There were no histories of fractures, angular deformities or forelimb lameness. 12.5% of the dogs included in the study were mixed breed, the remaining were dogs of pure breed ranging from Minipoodle to Rottweiller.

Determination of the body and of the bone mass

Body mass was determined on a standard balance with a precision of 0.5 kg. The forearms were then harvested and soft tissues were removed. The left radii were released from the ulnae by cutting the interosseous membrane, the ligamentous and the capsular tissues and radial bone mass was determined with a balance with a precision of 0.01 g. Bones were then wrapped in saline-soaked towels and frozen at −20 °C until further measurements were taken. They defrosted at room temperature (23 °C) and wrapped in saline-soaked gauze during each evaluation.

Computed tomography (CT)

The right radii and ulnae, anatomically attached, were examined by CT using standard software. The machine (GE lightspeed plus, Wisconsin, USA) was calibrated in accordance with the manufacturer's instructions. Its settings were 140 kV, 40 mA, with time set at 1.4 s. Slice thickness was set to 1.25 mm and interscan thickness to 1.25 mm. Each forearm was positioned with the mechanical axis of the radius parallel to the direction of the scan and perpendicular to the rays. The mechanical axis was defined as the line connecting the center of the loading surface in the proximal and distal articulation. It passes through the center of the radial head and the middle of the interfossa ridge, between the interfossa and the lunatae fossae on the distal radial surface [32]. Image matrix size was 512×512 pixels and the field of view was 12.0×12.0 cm. Images were saved in DICOM format.

Calculation of the radial geometrical properties

Radius slices were converted into the IGES extension with the Mimics (Materialise's Interactive Medical Control System) 6.3 software (Materialise NV 1999). The Rhinoceros 2.0 software (Robert McNeel and Associates, Seattle, WA) was employed to create a surface for each slice and a 3D model was created for each radius by lofting the surfaces. The mechanical axis of the bone was drawn for each 3D model. The geometrical properties of interest were: the radial length (mm), the total volume of the bone (cm^3) and the cortical and spongy volume percentages. The slice located at 50% of the distoproximal radial length (the 50% slice) of each radius was chosen to enter a simplified beam model and their cross-sectional properties were determined in order to qualitatively appraise their surface stresses. The cross-sectional geometrical properties of interest were: $B.Di_{(m-l)}$, the bone diameter (mm) in medial–lateral direction; $B.Di_{(a-p)}$, the bone diameter (mm) in anterior–posterior direction; Ps. Ar, the outer area (defined as the area bounded by the periosteum); Me.Ar, the area of medullary cavity; CSA, the cross-sectional area (mm^2); the moment of inertia (mm^4) with respect to a mediolateral axis (I_{ap}) and an anteroposterior axis (I_{ml}) passing through the centroid; the polar moment (I_p) of inertia (mm^4) with respect to the centroid; the width (mm) of the four cortices ($Ct.Wi_{ant}$, $Ct.Wi_{post}$, $Ct.Wi_{med}$, $Ct.Wi_{lat}$) along this axes; $Ct.Wi_{mean}$, the mean cortical thickness (mm) and the distance (mm) between the 50% slice's centroid and the mechanical axis. The surface (mm^2) of the radial head and the distal radial articular surface (mm^2) were also calculated. All measurements were performed with Rhinoceros 2.0 on a Pentium 4.2, 8 GHz, computer by the same operator.

The same cross-sectional geometrical properties of other three sections of the distal radius were retrieved from our previous paper [7] and entered in the linear regression model once validated with the measurements obtained with Rhinoceros 2.0.

Dual-energy X-ray absortiometry

Cranial–caudal scans of the left radii were made with a Hologic QDR-4500A and the Low Density Spine software (Hologic Inc., Waltham, MA 02154, U.S.A.). The machine was calibrated according to the manufacturer's instructions. Its settings were 140/100 kVp, 2.5 mA. Scan length was 20.362 cm, width of scan was 11.357 cm, line spacing was 0.1008 cm and point resolution was 0.0901 cm. Each radius was positioned in pronation with

the mechanical axis parallel to the direction of scan and normal to the rays. The scans were performed distal-proximally in a plexiglass box. Simulation of soft tissues was obtained by placing the bones in 5 cm of water according to the manufacturer's instruction. Repeatability was evaluated by taking three consecutive measurements of three samples with repositioning of both the sample and the laser beam; the coefficient of variation (CV) was calculated. The same operator positioned all the samples. The entire bone mineral content (BMC) was calculated.

Mechanical testing

The failure properties of these right radii were tested in axial compression with a Schenck machine (Schenck Trebel RSA 100, 50 Hz, 100 kN, Ulm, Germany) calibrated according to the manufacturer's instructions.

Bones were manually positioned upside down by the same operator with the mechanical axis at right angles to the ground (Fig. 1). The radius is thought to function as a thin beam restrained distally and proximally with a hinge. To partially avoid shear stresses due to the end effect created by machining the bones, thin custom hard rubber jigs were used to spread the load evenly over the proximal and distal joint surfaces. They held the bones in position and restrained the joint surface for mediolateral and anteroposterior translations without preventing torsion of the entire bone and rotation of the epiphysis around a mediolateral axis passing through the articular plane. The rubber jigs leaned on sandpapers glued on the plates. The machine was programmed in three steps. In the first, the plates were moved closer at 50 mm/min until a 19 N load was reached. The second step now brought them closer at a constant 400 mm/min until failure. This displacement rate was set in order to dump the viscous effects, restrain as physiologically as possible and prevent any mechanical adaptation of bone (creep, relaxation and hysteresis) during the test. The behavior, restraint and position of the samples were followed during the test. When the load cell detected a load below 5 N, the third step returned the plates to their starting position. A load cell continuously recorded the reaction force produced by the sample as the average of four values per millisecond (acquisition rate 4 MHz). A load–displacement curve was plotted for each sample. Samples unsuccessfully tested because of bad restrain fracture or uncompleted data acquisitions were discarded.

The beam model

Each bone was likened to a thin beam in view of the consistency of their length:diameter ratio and of their behavior observed during the test. The models were built for each bone starting from its radial geometrical properties and linked with their mechanical characteristics. Although the loading pattern of a long bone is very complex, in view of the behavior observed during the test and of previous studies [12,28,48] relevant loading patterns were assumed to be axial compression and bending. The 50% slice was assumed to lie at right angles to the mechanical axis during the bone strain. The surface stresses on this slice were calculated from the compressive force and the bending moment in two conditions (Fig. 2). Condition (a): the bone is loaded with the entire weight of the animal and assumed to be unstrained with respect to the condition acquired with the CT scans. The maximum stress on the surface of the 50% slice was defined as the static stress. Condition (b): the bone is loaded with the ultimate load and strained as determined by means of the mechanical test. The highest stress on the surface of the 50% slice at the ultimate load was called the ultimate stress and defined as σ maxima (σ_{max}). This same tension was assumed to be bearable by the tissue and, called σ admissible (σ_{adm}), considered as a macroscopical bone material property. Under the artificial assumption of bone as an isotropic homogeneous material, the strains of the tissue located on the surface of the 50% slice can be extrapolated from those estimated stresses and the elastic modulus. The compressive force and bending moment were derived from the data collected in our test and measurements.

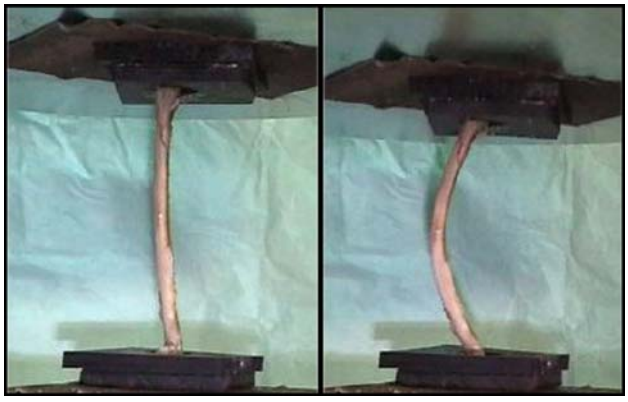

Fig. 1. The first step of the axial compressive test and the last frame before the failure point. The radius is thought to function as a thin beam restrained distally and proximally with a hinge. Thin custom hard rubber jigs were used to spread the load evenly over the proximal and distal joint surfaces. They held the bones in position and restrained the joint surface for mediolateral and anteroposterior translations without preventing torsion of the entire bone and rotation. The compliance of the rubber jigs was ascertained and their individual effect on the displacement was taken into account for each sample.

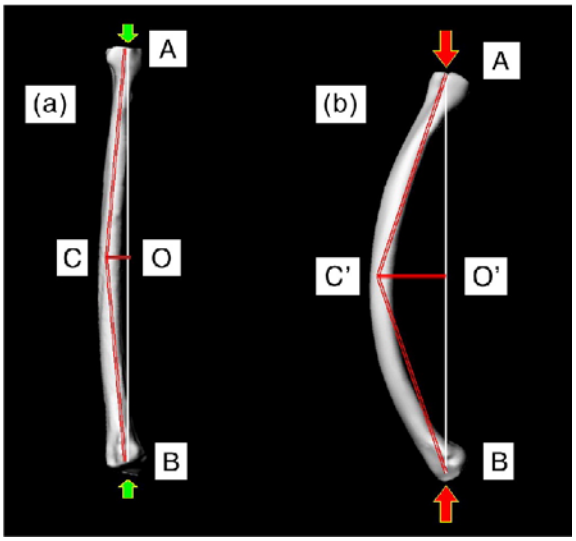

Fig. 2. The beam model of the sample shown in Fig. 1. Stresses on the cross-section located at the 50% of the distoproximal radial length were calculated in two conditions: (a) the radius is bearing the animal's whole weight, (b) the radius is at the ultimate load and ultimate displacement detected during the biomechanical test. The effects of the compressive load and the bending moment were calculated as (a) static stress and (b) failure stress (σ_{max}). CO = static lever arm; C′O′ = failure lever arm; AB = mechanical axis.

Data analysis

The mean bone mineral density (BMD) (g/cm^3) was calculated for each sample as the DXA-detected BMC and the 3D reconstruction total volume ratio. The slope of the elastic region, ultimate load (N), failure load (N) and ultimate displacement (mm) were recorded and the work to failure (J) and the normalized axial strain (%), were calculated from the load–displacement curve values (Fig. 3). The compliance of the rubber jigs was ascertained and their individual effect on the displacement was taken into account for each sample. The work to failure was calculated as the integral under the load–displacement curve until the failure load [57]. Normalized axial strain was calculated as the percentage ratio between the displacement at failure, less the rubber jigs effect, and the length of each bone. The amount of Newtons per unit of bone weight necessary to fracture was calculated as the ratio between the ultimate load (N) and the weight of the bone (N) and called as bone weights. The ratio between the ultimate stress and the static stress derived from the model was calculated as a safety index.

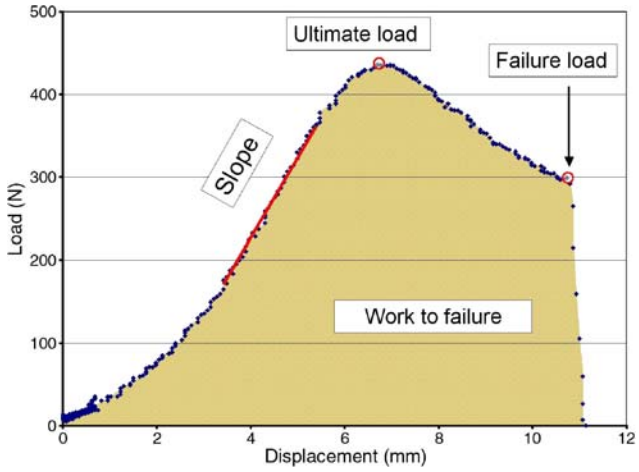

Fig. 3. The load–deformation curve relative to the sample examined and the parameters inferred: the slope of the elastic region (N/mm), ultimate load (N), failure load (N) and displacement (mm) were recorded and the work to failure (J) and the normalized axial strain (%) were calculated from the load–displacement curve values.

Allometric equations

Scaling of the bone mass with the body mass and that of the geometrical, densitometric and the mechanical properties of the radius with the bone mass was investigated. A typical power function $Y = Y_0 M^b$ was chosen to determine how a hierarchical tissue organizes itself when facing two orders of magnitude. The theoretical exponents were determined by dimensional analysis assuming self-similarity of the geometry, and the mechanical tests according to classic elastic solutions: ultimate and failure loads proportional to a moment of inertia over the square of a length (of the bone); displacement proportional to a length; slope of the elastic region proportional to load over displacement; work to failure proportional to load times displacement; strain as percentage; safety index proportional to load over mass; stress (σ) proportional to strain.

Statistical analysis

Statistics were calculated with the SPSS 12.0 and $p < 0.05$ as the significance cut-off. One-way ANOVA was used to analyze the gender distribution of geometrical, densitometric and mechanical bone features. Fracture distribution between the sexes was analyzed with the χ^2 test. A multiple linear regression analysis with stepwise analyses was performed to determine which parameters rule a bone's mechanical function. Sequential Bonferroni post hoc adjustment of the p-values was used. The effects of the animal mass on the mean BMD and on the σ_{max} were determined by means of a linear regression analysis. The relationships between the bone mass and the parameters investigated were analyzed by means of a model II regression in order to state how the scaling of the bone characteristics acts on its mechanical behavior. The log-transformed variables were regressed against log bone mass using the reduced major axis (RMA) technique and 95% confidence intervals on their empirical estimates were calculated. The null hypothesis, that dimensional analysis on the assumption of geometrical self-similarity and mechanical testing according to classic elastic solutions are not reasonable in bones, was rejected when the expected theoretical values fell within the 95% confidence intervals.

Results

The DXA measurement CV was 0.4%. Bones were observed to fail in bending and samples successfully tested had diaphyseal or proximal metaphyseal fracture. 71.4% of the fractures were single, 28.6% were multiple with various configurations generally located closer to the radial head. Single fractures were diaphyseal or proximal metaphyseal, all transverse or short oblique. The fracture distribution was not significantly influenced by mass or sex. The profiles of the load–displacement curves were consistent with the test and their pattern was always similar.

Table 1
Results of ANOVA with mean and standard deviations for the mechanical bone properties, the cortical volume percentage, the bone mineral density (BMD) and the bone mineral content (BMC) as distributed according to sex

	Female (18)	Males (14)	p
Ultimate load (N)	1185.27±727.22	2066.5±1470.86	NS
σ_{max} (MPa)	455±103.21	584.1±135.65	0.015
Work to failure (J)	7.8±5.2	14.1±9.8	0.047
Cortical volume percentage (%)	0.625±0.037	0.592±0.045	0.037
BMD (g/cm^3)	1.08±0.31	1.24±0.51	NS
BMC (g)	8.7±7.02	11.22±9.58	NS

The one-way ANOVA revealed a significant gender difference in the mechanical bone features with no differences in BMD. The female bones had a higher cortical bone volume percentage. The male bones required more energy to fracture and our model shows that their tissue fails at a greater tension (σ_{max}) (Table 1). The σ_{max} was influenced by the percentage of cortical vs. spongy bone (0.002). The sequential Bonferroni adjusted linear regression model demonstrated that the parameters representative of the bone mechanical behavior are well

Table 2
A multiple linear regression analysis with stepwise analyses performed to determine which parameters rule each bone mechanical feature

	Standardized beta	T	p
Dependent variable: ultimate load (R^2 0.98)			
I_p 40%	1.53	7.47	0.000
Dependent variable: failure load (R^2 0.98)			
I_p 30%	1.17	12.15	0.000
CSA 20%	−0.60	−3.72	0.002
Dependent variable: slope (R^2 0.93)			
I_p 40%	0.96	14.47	0.000
Dependent variable: work to failure ($R^2$1.000)			
I_{ap} 40%	0.55	9.881	0.000
C_{post} 50%	−0.16	−9.360	0.000
Ct.Wi$_{mean}$ 50%	0.360	6.037	0.000
Animal mass	0.23	6.869	0.000
B.Di$_{(a-p)}$ 50%	−0.642	−6.884	0.000
Sex	0.036	4.609	0.001
Age	0.023	3.632	0.003
Dependent variable: bone weights ($R^2$0.87)			
Bone mass	−4.033	−9.095	0.000
Cortical bone volume	3.198	7.849	0.000
Ct.Wi$_{ant}$ 50%	0.614	4.859	0.000
Sex	0.296	3.128	0.006
Dependent variable: σ_{max} ($R^2$0.60)			
Sex	0.479	3.220	0.005

Sequential Bonferroni post hoc adjustment of the p-values was used reducing the significance cut-off of the p-value to $p < 0.00625$. See nomenclature on Materials and methods.

predicted by BMC, bone cross-sectional and three-dimensional geometrical properties, sex and body mass (Table 2). The animal mass was found not to significantly influence the mean bone mineral density (NS) and σ_{max} (NS).

Results of the reduced major axis regression and 95% confidence intervals of the log mechanical features and the log three-dimensional geometry with the log bone mass are summarized in Table 3. Those expressing the log–log regression of the geometrical properties of the cross-section located at 50% of the distoproximal radial length with the bone mass are summarized in Table 4. Results of the same regressions performed on the 20, 30 and 40% cross-sections were truly comparable and are not reported.

Concerning the macroscopic bone material features, the bone mass was found to scale almost linearly with the animal mass (s=0.949). The BMC (g) was found to scale almost linearly with the animal mass (s=1.004) while the mean BMD (g/cm^3) was found to be mass invariant. A close fit was found between the experimentally determined and the theoretical slopes (according to classic elastic solutions) concerning the mechanical features. In particular the work to failure was found to scale almost linearly with the bone mass (s=0.926). The estimated admissible tension (and thus the admissible strain) and normalized axial strain were found to be mass invariant (s=0.006, s=0.068). The safety index was found to decrease with the increase of bone mass (s=−0.343). The bone length (mm) was found to increase much less than proportionally with increasing mass (s=0.329) while the total bone volume and the volume dedicated to cortical and spongy bone were found to scale almost linearly with the bone mass (s=0.916, s=0.885, s=0.971).

Scaling of the cross-sectional geometrical properties of all the parameters investigated was found to be similar in all the four sections analyzed. Cortices width (Ct.Wi$_{ant}$, Ct.Wi$_{post}$, Ct.Wi$_{med}$, Ct.Wi$_{lat}$) and mean cortical thickness (Ct.Wi$_{mean}$) were found to scale slowly with the bone mass (s ranging: 0.235–0.298). The area of the medullary cavity (Me.Ar) was found to scale faster (s range: 1.583–1.700) than (Ps.Ar) the outer area (s range: 0.759–0.779) so that the cross-sectional area (CSA) was found to scale as expected with mass$^{2/3}$. Moments of inertia (I_{ml}, I_{ap}, I_p) were found to scale slightly faster than the expected mass$^{4/3}$.

Table 3
Results of the reduced major axis (RMA) regression and 95% confidence limits expressing the scaling of the log inquired features with the log bone mass

	M=bone mass					
Variable	Intercept	s (exper)	$s*$ (theor)	R	Confidence limits	
Animal's mass (kg)	2.726	0.949	1	0.915	0.836	1.067
Bone mineral content and mean bone mineral density						
Bone mineral content (g)	2.653	1.004	1	0.931	0.919	1.102
Mean BMD (g/cm^3)	0.247	0.112	0	0.334	−0.009	0.492
Mechanical test						
Ultimate load (N)	4.498	0.812	2/3	0.963	0.726	0.894
Failure load (N)	4.484	0.862	2/3	0.959	0.754	0.955
Ultimate load/bone weight	3.291	−0.309	−1/3	−0.705	−0.405	−0.218
Displacement (mm)	1.497	0.278	1/3	0.843	0.217	0.323
Slope elastic region (N/mm)	3.448	0.645	1/3	0.938	0.543	0.734
Work to failure (J)	2.484	0.926	1	0.940	0.816	1.065
Normalized axial strain	0.756	−0.068	0	−0.343	−0.149	−0.011
Safety index differential scaling	3.354	−0.343	−1/3	0.498	−0.484	−0.220
σ_{max} (MPa)	2.703	0.006	0	0.022	−0.114	0.099
3D—geometry						
Bone length (mm)	2.711	0.329	1/3	0.909	0.293	0.374
Bone volume (cm^3)	2.461	0.916	1	0.918	0.799	1.034
Cortical volume (cm^3)	2.189	0.885	1	0.922	0.782	0.996
Spongeous volume (cm^3)	2.149	0.971	1	0.906	0.832	1.107

The theoretical slopes ($s*$) have been determined by dimensional analysis on the assumption of geometrical self-similarity and according to classic elastic solutions. The fit between the experimentally determined and the theoretical slopes is close. Most of the expected theoretical values fell within the 95% confidence intervals. Dimensional analyses on these assumptions are then reasonable in bones tested in accordance to our set up.

Table 4
The log transformed geometrical variables of the cross-section located at the 50% of the distoproximal radial length regressed against log bone mass using the reduced major axis (RMA) technique and 95% confidence intervals on their empirical estimates

	M=bone mass					
	Cross-sectional properties 50%					
Variable	Intercept	s (exper)	$s*$ (theor)	R	95% confidence limits	
B.Di$_{(m-l)}$	1.710	0.366	1/3	0.960	0.335	0.390
B.Di$_{(a-p)}$	1.620	0.417	1/3	0.960	0.380	0.456
Ct.Wi$_{med}$	1.050	0.298	1/3	0.550	0.224	0.369
Ct.Wi$_{lat}$	0.889	0.235	1/3	0.530	0.184	0.286
Ct.Wi$_{ant}$	0.836	0.263	1/3	0.570	0.190	0.333
Ct.Wi$_{post}$	0.808	0.254	1/3	0.624	0.177	0.317
Ct.Wi$_{mean}$	0.829	0.260	1/3	0.778	0.205	0.314
Ps.Ar	3.222	0.779	2/3	0.970	0.717	0.837
Me.Ar	3.993	1.700	2/3	0.903	1.406	1.994
CSA	2.894	0.645	2/3	0.948	0.582	0.717
I_{ml}	5.156	1.566	4/3	0.965	1.432	1.700
I_{ap}	5.325	1.460	4/3	0.967	1.341	1.570
I_p	5.534	1.490	4/3	0.968	1.366	1.603

The same regression performed on cross-sections located at 20, 30 and 40% of the distoproximal radial length demonstrated truly comparable results and is not reported. The theoretical slopes ($s*$) have been determined by dimensional analysis on the assumption of geometrical self-similarity. See nomenclature on Materials and methods. The area of the medullary cavity (Me.Ar) was found to scale faster than (Ps.Ar) the outer area so that the cross-sectional area (CSA) was found to scale as expected with mass$^{2/3}$. Moments of inertia (I_{ml}, I_{ap}, I_p) were found to scale slightly faster than the expected mass$^{4/3}$.

Discussion

The weights of terrestrial mammals embrace roughly six orders of magnitude, but are borne by substantially the same molecular structures hierarchically organized at a supramolecular, microstructural and macrostructural level to endure the

mechanical loads generated by physiological activity [1]. The purpose of our research was to quantitatively evaluate how bone tissue arranges itself macroscopically in order to optimally face appreciable changes in size. This subject was investigated within a single species, the canine species, to avoid possible misleading results due to between-species bone tissue and macroscopic limb posture differences. Domestication of dogs has been followed by selective breeding to obtain mighty animals for hunting and toy dogs as pets, with a consequent weight range of 1.5 to 70 kg and a unique 40-fold difference in body mass. Examination of bones from a set of breeds with a common genetic ancestry [61] can thus give an idea of how their tissue adapted to cope with such a wide range of functional requirements.

Forelimbs were chosen because they bear most of the static and dynamic loads and the forearms posture is similar regardless of the considered breeds. The easiest loading pattern within these limbs was recognized to be the radial one. In outline the ulna and the ligamentous and the muscular tissues between the two bones work in order to enable the radius to be loaded in axial compression. Controlateral limbs were tested for different features as previous studies had validated [38,39].

Plotting and inferring its load-deformation curve during loading under controlled conditions can determine the main mechanical properties of a bone. As variations in size, shape or composition are able to drastically change a bone's strength, stiffness or energy absorption capacity [59], we choose for a whole bone structural test. In view of the previous anatomical remarks, the test was set in axial compression. Data derived from such test were taken in account for the whole features at once. Matching the biomechanical properties with the material and structural characteristics of each sample and determining how they scale with mass has shown which attributes vary in order to curb the energy effects of an animal mass increase.

The mechanical test showed that the work to failure scales almost linearly with bone mass. This crucial finding means that bones of different sizes require a mass invariant amount of energy per unit of mass to failure. This outcome is reached through a different structural behavior according to our test. The difference was not found in the normalized axial strain or in the strains estimated by means of our model scaling, which were found to be almost mass invariant, but in the scaling of the ultimate and failure load and in the slope of the elastic region.

The different behavior could be attributed both to the material properties and to the geometrical properties. Our findings, in agreement with previous studies [8,12,28] provide information on the material properties of the bone within a species: the almost linear scaling of the BMC and bone mass reveals that the amount of material "bone tissue" employed is basically linked with the body mass and that the two-phase ratio is substantially constant. The independence of the BMD (g/cm^3) and failure stress from the bone mass suggests that under a single axial load the macroscopical material properties of bones within a species are the same irrespective of its size. The bricks used to build a part of the bearing framework of a healthy individual within species are mass invariant according to our test and possess macroscopically the same material properties in bones of different size. Our BMD results are in line with those observed (g/cm^2) in greyhounds [39]. Concerning the geometrical properties, interestingly the analysis of the allometric equations showed that as the animal mass increases bones proportionally distribute their tissue further from the cross-sectional centroid achieving an effective increase in the cross-sectional moments of inertia. This layout is reached employing an amount of tissue proportional to the animal mass, reducing proportionally the bone length, maintaining essentially constant the width of the cortices and acting on the medullary cavity and the outer area scaling.

Matching the results of the multiple linear regression model on the biomechanical properties with the scaling of the material and structural characteristics, this different three-dimensional arrangement is believed to enable bones of different size to absorb a proportional amount of energy before failure. In accordance with our simplified beam model, it leads to the development of similar stresses and strains on the cross-sections facing increasing loads. If the molecular structures of the hierarchically organized bone tissue need macroscopically a fixed amount of Joule per unit of mass to become disorganized and fail, the bone structures need to be redesigned in order to curb the energy effects of the size increase. An efficient and energetically economic solution is to alter the three-dimensional layout employing an amount of tissue proportional to the animal mass. The different arrangement influences the bones behavior in their pathway to failure. Even though the bone mechanical competence was found to be mass related, the energy effects of increased body size can be appreciated in the slightly negative trend of the scaling of the safety index with mass: large animals are in spite of everything potentially closer to fracture than smaller ones. This size effect is due to the higher static stresses.

Gender differences in bone mechanical properties irrespective of body mass thus evident in the same species are neither due to a different BMC, nor to cortical cross-sectional differences. Our results show they are the consequence of macro architectural dissimilarities in the ratio between the amounts of tissue invested in cortical and spongy bone. It is reasonable to presume that gender-assigned bone structures, composed of different percentage of these tissues, each with its elastic modulus, have different mechanical features being nevertheless competent with respect to the animal size.

There is a close fit between the experimentally determined and the theoretical slopes of the log regressed allometric equations. Most of the expected theoretical values fell within the 95% confidence intervals. Dimensional analysis on the assumption of geometrical self-similarity and mechanical testing according to classic elastic solutions are then reasonable in bones tested in accordance to our set up.

The work to failure scaling indicates that energy is dissipated in a fractal domain, probably related to the hierarchical bone structure, with dimension ~ 2.8 (0.926×3), thus intermediate between that of a Euclidean surface and a volume [21].

This study has several limitations. The morphology of the radius and its mechanical properties were assessed outside the context of the ulna and the surrounding tissues. Their action may contribute to increase the ability of the forearm to curb the

energy effect of a size increase reducing the importance of the allometric changes here highlighted. The bone material properties were inferred from a macroscopical point of view determining a mean bone mineral density regardless of the localization and estimating the stresses and strains on specific cross-sections through a simplified model. These mostly qualitative results are necessarily inaccurate but show, however, a trend that could be further inquired with more accurate models.

In conclusion, this research demonstrates that bone geometry is the parameter that macroscopically rules the mechanical function of this tissue. Its allometric changing is the strategy a bone adopts to adjust its structure and function to compensate for the physical consequences of differences in size. This adjustment is efficiently and economically reached redistributing an amount of tissue proportional to the animal mass so that the energy per unit of mass necessary to fracture a bone remains mass invariant. According to a simplified beam model, it leads to the development of similar stresses and strains on the cross-sections facing increasing loads. The percentage of bone volume allocated to the cortical and spongeous portion was found to be a gender difference responsible for a different mechanical behavior. These results illustrate how the bone tissue approaches optimum efficiency linked with the animal gender and size and the relative energetic and stressing consequences acting on the morphological features.

Acknowledgments

The authors are grateful to “Tecnologie Avanzate” (Italy) for the kind gift of the spine low density software.

References

[1] Akkus O, Yeni YN, Wasserman N. Fracture mechanics of cortical bone tissue: a hierarchical perspective. Crit Rev Biomed Eng 2004;32(5–6): 379–426.
[2] Alexander RMcN. Allometry of limb bones of mammals from shrews (Sorex) to elephant Loxodonta. J Zool (Lond) 1979;189:305–14.
[3] Alexander RMcN. Animal mechanics. 2nd ed. Oxford: Blackwell; 1983.
[4] Arrhenius O. Species and area. J Ecol 1921;9:95–9.
[5] Biknevicius AR. Biomechanical scaling of limb bones and differential limb use in caviomorph rodents. J Mammal 1993;74:95–107.
[6] Back P. How nature works. New York: Springer-Verlag; 1996.
[7] Brianza SZM, Delise M, Maddalena Ferraris M, D’Amelio P, Botti P. Cross-sectional geometrical properties of distal radius and ulna in large, medium and toy breed dogs. J Biomech 2006;39(2):302–11.
[8] Biewener AA. Bone strength in small mammals and bipedal birds—Do safety factors change with body size? J Exp Biol 1982;98:289–301.
[9] Biewener AA. Allometry of quadrupedal locomotion: the scaling of duty factor, bone curvature and limb orientation to body size. J Exp Biol 1983; 10S:147–71.
[10] Biewener AA. Mammalian terrestrial locomotion and size. BioScience 1989;39:776–83.
[11] Biewener AA. Biomechanics of mammalian terrestrial locomotion. Science 1990;250:1097–103.
[12] Biewener AA. Musculoskeletal design in relation to body size. J Biomech 1991;24:19–29.
[13] Biewener AA. Biomechanical consequences of scaling. J Exp Biol 2005; 208:1665–76.
[14] Brody S. Bioenergetics and growth. New York: Reinhold; 1945 (Reprint. Darien, CT: Haffner 1964).
[15] Burlando B. The fractal dimension of taxonomic systems. J Theor Biol 1990;146:88–114.
[16] Burlando B. The fractal geometry of evolution. J Theor Biol 1993;163: 161–72.
[17] Brown JH. Macroecology. Chicago, IL: The University of Chicago Press; 1995.
[18] Brown JH, West GB, Enquist BJ. Scaling in Biology. Oxford University Press; 2000.
[19] Brown JH, West GB, Enquist BJ. Scaling in biology: patterns and processes, causes and consequences. Scaling in Biology. Oxford University Press; 2000. p. 4–5.
[20] Brown JH, West GB, Enquist BJ. Scaling in biology: patterns and processes, causes and consequences. Scaling in Biology. Oxford University Press; 2000. p. 1–2.
[21] Carpinteri A, Pugno N. Are the scaling laws on strength of solids related to mechanics or to geometry? Nat Mater 2005;4:421–3.
[22] Casinos A, Bou J, Castiella MJ, Viladiu C. On the allometry of long bones in dogs (*Canis familiaris*). J Morphol 1986;190:73–9.
[23] Christiansen P. Mass allometry of the appendicular skeleton in terrestrial mammals. J Morphol 2000;251:195–209.
[24] Damuth J. Population and body size in mammals. Nature 1981;290: 699–700.
[25] Damuth J. On size and abundance. Nature 1991;351:268–9.
[26] Demes B, Junger WL, Selpien K. Body size, locomotion, and long bone cross-sectional geometry in indriid primates. Am J Phys Anthropol 1991; 86:537–47.
[27] Dodds PS, Rothman DH, Weitz JS. Re-examination of the ‘‘3/4-law’’ of metabolism. J Theor Biol 2001;209:9–27.
[28] Garcia GJM, da Silva JKL. On the scaling of mammalian long bones. J Exp Biol 2004;207:1577–84.
[29] Gasc J. Comparative aspects of gait, scaling and mechanics in mammals. Comp Biochem Physiol, Part A 2001;131:121–33.
[30] Hanna JB, Polk JD, Schmitt D. Forelimb and hindlimb forces in walking and galloping primates. Am J Phys Antropol 2006;130:529–35.
[31] Hochachka PW, Darveau CA, Andrews RD, Suarez RK. Allometric cascade: a model for resolving body mass effects on metabolism. Comp Biochem Physiol, Part A 2003;134:675–91.
[32] Hsu ES, Patwardhan AG, Meade KP, Light TR, Martin WR. Cross-sectional geometrical properties and bone mineral contents of the human radius and ulna. J Biomech 1993;26(11):1307–18.
[33] Huxely JS. Problems of relative growth. London: Methuen; 1932.
[34] Iriarte-Díaz J. Differential scaling of locomotor performance in small and large terrestrial mammals. J Exp Biol 2002;205:2897–908.
[35] Kleyber M. Body size and metabolism. Hilgardia 1932;6:315–53.
[36] Li JK-J. Comparative cardiovascular dynamics in mammals. Boca Raton, FL: CRC Press; 1996.
[37] Li JK-J. A new approach to the analysis of cardiovascular function: allometry. In: Drzewieky G, Li J K-L-, editors. Analysis of cardiovascular function. New York: Springer-Verlag; 1998. p. 13–29.
[38] Markel MD, Sielman E, Rapoff AJ, Kohles SS. Mechanical properties of long bones in dogs. Am J Vet Res 1994;55(8):1178–83.
[39] Markel MD, Sielman E, Bodganske JJ. Densitometric properties of long bones in dogs, as determined by use of dual-energy X-ray absorptiometry. Am J Vet Res 1994;55(12):1750–6.
[40] McMahon T. Size and shape in biology. Science 1973;179:1201–4.
[41] McMahon T. The mechanical design of trees. Sci Am 1975;233(1): 92–102.
[42] McMahon T. Allometry and biomechanics: limb bone in adult ungulates. Am Nat 1975;109:547–63.
[43] McMahon TA. Using body size to understand the structural design of animals: quadrupedal locomotion. J Appl Physiol 1975;39:619–27.
[44] McMahon T, Kronauer RE. Tree structures: deducing the principle of mechanical design. J Theor Biol 1976;59:443–66.
[45] McMahon T, Bonner JT. On size and life. New York: Scientific American Books; 1983.
[46] Murray CD. The physiological principle of minimum work: I. The vascular system and the cost of blood volume. Proc Natl Acad Sci U S A 1926; 12:207–14.

[47] Peters RH. The ecological implications of body size. Cambridge, U.K: Cambridge Univ. Press; 1983.
[48] Rubin CT, Lanyon LE. Dynamic strain similarity in vertebrates; an alternative to allometric limb bone scaling. J Theor Biol 1984;107: 321–7.
[49] Schaffler MB, Burr DB. Primate cortical bone microstructure: relationship to locomotion. Am J Phys Anthropol 1984;65:191–7.
[50] Schaffler MB, Burr DB, Jungers WL, Ruff CB. Structural and mechanical indicators of limb specialization in primates. Folia Primatol 1985;45(2): 61–75.
[51] Smidt-Nielsen K. Scaling, why is animal size so important? Cambridge: Cambridge University Press; 1984.
[52] Schmitt D. Compliant walking in primates. J Zool (Lond) 1999;248: 149–60.
[53] Taylor CR, Schmidt-Nielsen K, Raab JL. Scaling of energetic cost of running to body size in mammals. Am J Physiol 1970;219:1104–7.
[54] Taylor CR, Heglund NC, Maloiy GMO. Energetics and mechanics of terrestrial locomotion: I. Methabolic energy consumption as a function of speed and body size in birds and mammals. J Exp Biol 1982;97:1–21.
[55] Thompson D'AW. On growth and form. Cambridge: Cambridge Univ. Press; 1917.
[56] Toro E, Herrel A, Vanhooydonck B, Irschick DJ. A biomechanical analysis of intra- and interspecific scaling of jumping and morphology in Caribbean Anolis lizards. J Exp Biol 2003;206:2641–52.
[57] Turner CH, Burr DB. Experimental techniques for bone mechanics. In: Cowin SC, editor. Bone mechanics handbook. Boca Raton, FL: CRC Press; 2001. p. 7.6–7.
[58] Van Der Meulen MCH, Carter DR. Developmental mechanics determine long bone allometry. J Theor Biol 1995;172:323–7.
[59] Van Der Meulen MCH, Jepsen KJ, Mikic' B. Understanding bone strength: size isn't everything. Bone 2001;29:101–4.
[60] Wayne RK. Limb morphology of domestic and wild canids: the influence of development on morphologic change. J Morphol 1986;187:301–19.
[61] Wayne RK, Ostrander EA. Origin, genetic diversity, and genome structure of the domestic dog. BioEssays 1999;21:247–57.
[62] Weibel ER, Taylor CR, Bolis L, editors. Principles of animal design. The optimisation and symmorphosis debate. Cambridge, MA: Cambridge University Press; 1998.
[63] West GB, Brown JH, Enquist BJ. A general model for the origin of allometric scaling laws in biology. Science 1997;276:122–6.
[64] West GB, Brown JH, Enquist BJ. The fourth dimension of life: fractal geometry and allometric scaling of organisms. Science 1999;284:1677–9.